Parameter Estimation and Identifiability in Bistatic Multiple-Input Multiple-Output Radar

FRANKIE K. W. CHAN
Shenzhen University
Shenzhen, China

H. C. SO, Fellow, IEEE
City University of Hong Kong
Hong Kong, China

LEI HUANG, Senior Member, IEEE
Shenzhen University
Shenzhen, China

LONG-TING HUANG
City University of Hong Kong
Hong Kong, China

An iterative ESPRIT-like algorithm is devised for direction-of-departure (DOD) and direction-of-arrival (DOA) estimation in multiple-input multiple-output radar. Our proposal can handle identical DODs and DOAs, and provides autopairing of the angle parameters. Furthermore, it is proved that the multiple signal classification methodology cannot identify ($MN - 1$) targets, where M and N are the element numbers in the transmit and receive antennas, respectively. Simulation results are included to evaluate the performance of the proposed algorithm.

Manuscript received July 26, 2013; revised March 17, 2014, December 8, 2014; released for publication February 15, 2015.

DOI. No. 10.1109/TAES.2015.130502.

Refereeing of this contribution was handled by G. San Antonio.

The work described in this paper was in part supported by the NSFC/RGC Joint Research Scheme sponsored by the Research Grants Council of Hong Kong and the National Natural Science Foundation of China (Project N CityU 104/11, 61110229/61161160564), and by the National Natural Science Foundation of China (61222106).

Authors' addresses: F. K. W. Chan, L. Huang, College of Information Engineering, Shenzhen University, Shenzhen 518060, China; H. C. So, L.-T. Huang, Department of Electronic Engineering, City University of Hong Kong, Tat Chee Avenue, Kowloon, Hong Kong SAR. Corresponding author is L. Huang, Email: (lhuang8sasp@hotmail.com).

I. INTRODUCTION

Multiple-input multiple-output (MIMO) radar has received considerable attention recently [1–3]. Unlike the traditional phased array radar, the MIMO radar is able to utilize multiple transmit and receive antennas for transmitting and receiving signals. Moreover, the transmitter simultaneously sends out orthogonal waveforms, which leads to gain of waveform diversity. In the presence of targets, the transmitted signal will be reflected to the receiver. The MIMO radar is superior to the phased array radar in target detection because the former transmits a wide beam while the latter uses a narrow beam for probing targets. As a result, the MIMO radar can offer better parameter identifiability and resolution [4].

In statistical MIMO radar [5–7], the transmit antennas are widely separated and the targets can be identified from different angles at the same time. As a result, spatial diversity of the system is increased by exploiting different radar cross section (RCS) information, and targets can be detected and located with high resolution. Unlike the statistical radar, the transmit antennas of colocated MIMO radar are very close to each other. Hence, the RCSs of the targets can be treated equal. Colocated MIMO radar can be categorized into two types, namely, monostatic and bistatic. For monostatic configuration, transmitters are close to the receivers, and thus the direction-of-departure (DOD) and direction-of-arrival (DOA) of each target are equal. It can provide higher parameter identifiability, more reliable target detection and more flexible transmit beam pattern design [8, 9]. On the other hand, the transmitters are far apart from the receivers in the bistatic radar, and hence each target has distinct DOD and DOA, resulting in improvement in covertness and localization accuracy [10].

In this paper, we focus on joint estimation of DODs and DOAs for K targets using a single pulse in bistatic MIMO radar. Unlike the existing estimation algorithms, the proposed algorithm is iterative and a function value checking procedure is used to ensure that the best DODs and DOAs estimates are selected. Therefore, the parameter estimate is guaranteed not worse than that of the commonly adopted estimation of signal parameters via rotational invariance techniques (ESPRIT) [11–13]. Here, the Swerling II model in which the distribution of RCS is fixed, is adopted. The DOD and DOA estimates correspond to the peak of the maximum likelihood (ML) cost function; though optimum, a $2K$-dimensional ($2K$-D) search is required. To alleviate the high computational burden, the search can be divided into $2K$ iterative 1-D searches [14] at the expense of slow convergence. Subspace algorithms such as the ESPRIT [11,12,15] and multiple signal classification (MUSIC) [16, 17], which exploit the signal and noise subspaces of the sample covariance matrix, are more computationally attractive and thus widely applied. In these suboptimal schemes, the DODs and DOAs are automatically paired up but the number of identifiable targets is less than that of the ML approach. The identifiability limit of the ESPRIT

algorithm is lower than that of the MUSIC method as the latter fully utilizes the noise subspace. In this paper, we propose an ESPRIT scheme that can offer more reliable parameter estimates than the conventional ESPRIT algorithm with higher identifiability limit. On the other hand, it has been claimed [18] that the MUSIC algorithm can identify up to $K = (MN - 1)$ sources where M and N are the numbers of elements in the MIMO radar transmit and receive antenna arrays. As the second contribution in this paper, we disprove this identifiability limit even for infinite snapshots.

The rest of the paper is organized as follows. In Section II, the signal model and problem formulation are introduced. The ESPRIT-like algorithm is developed in Section III. In Section IV, we prove that the MUSIC algorithm cannot identify $(MN - 1)$ targets. It is worth pointing out that this identifiability limit indicates the maximum number of identifiable targets, which is a necessary operational condition for the proposed method. In Section V, numerical examples are used to evaluate the performance of the proposed method. Finally, conclusions are drawn in Section VI.

Notation: We use boldface uppercase letters to denote matrices, boldface lowercase letters for column vectors, and lowercase letters for scalar quantities. Superscripts $(\cdot)^*$, $(\cdot)^T$, $(\cdot)^H$, $(\cdot)^{-1}$, and $(\cdot)^\dagger$ represent complex conjugate, transpose, Hermitian transpose, matrix inverse, and pseudo inverse, respectively. In addition, $\propto$ means proportional to. The $\hat{a}$ denotes the estimate of a and $\mathbb{E}\{a\}$ is the expected value of a. The $[\mathbf{A}]_{m,n}$ represents the (m, n) entry of $\mathbf{A} \in \mathbb{C}^{M\times N}$, while tr($\mathbf{A}$) and $|\mathbf{A}|$ are its trace and determinant, respectively. The diag($\mathbf{a}$) represents a diagonal matrix whose nonzero elements are given by $\mathbf{a}$ while the block diagonal matrix, with $\mathbf{A}_1$ and $\mathbf{A}_2$ being its components, is denoted by diag($\mathbf{A}_1$, $\mathbf{A}_2$). The vec($\mathbf{A}$) is the columnwise vectorized version of $\mathbf{A}$ with vec^{-1} being its inverse operator. The Kronecker product and Khatri-Roa matrix product are denoted by $\otimes$ and $\circ$, respectively. Furthermore, $\mathbf{I}_M$ is the $M \times M$ identity matrix, $\mathbf{0}_{M\times N}$ is the $M \times N$ zero matrix, and $\mathbf{1}_M$ is the $M \times 1$ vector with all elements equal one. The $\mathbf{x} \sim \mathcal{N}(\mu, \Sigma)$ means that $\mathbf{x}$ follows a complex Gaussian distribution with mean μ and covariance matrix $\mathbf{\Sigma}$.

II. SIGNAL MODEL AND PROBLEM FORMULATION

Consider a MIMO radar system consisting of M transmit and N receive antenna elements with uniform linear array (ULA) configuration. The reflected pulse of the K targets arrived at the receive antennas, after matched filtering, can be expressed as

$$\mathbf{X} = \mathbf{FS} + \mathbf{Q} \in \mathbb{C}^{MN\times L} \tag{1}$$

where

$$\mathbf{F} = \mathbf{H} \circ \mathbf{G} \in \mathbb{C}^{MN\times K} \tag{2}$$

$$\mathbf{G} = [\,\mathbf{g}_1 \quad \mathbf{g}_2 \quad \cdots \quad \mathbf{g}_K\,] \in \mathbb{C}^{M\times K} \tag{3}$$

$$\mathbf{H} = [\,\mathbf{h}_1 \quad \mathbf{h}_2 \quad \cdots \quad \mathbf{h}_K\,] \in \mathbb{C}^{N\times K} \tag{4}$$

$$\mathbf{g}_k = \begin{bmatrix} 1 & a_k & \cdots & a_k^{M-1} \end{bmatrix}^T \tag{5}$$

$$\mathbf{h}_k = \begin{bmatrix} 1 & b_k & \cdots & b_k^{N-1} \end{bmatrix}^T \tag{6}$$

$$a_k = \exp\left(j\frac{2\pi d_t \sin\left(\breve{\theta}_k\right)}{\lambda}\right) \tag{7}$$

$$b_k = \exp\left(j\frac{2\pi d_r \sin\left(\breve{\phi}_k\right)}{\lambda}\right). \tag{8}$$

The $\breve{\theta}_k \in (-\pi/2, \pi/2)$ and $\breve{\phi}_k \in (-\pi/2, \pi/2)$ denote the DOD and DOA of the kth target, respectively. Furthermore, λ is the carrier wavelength while d_t and d_r are the interelement separations in the transmitter and receiver, and they are known constants. The $[\mathbf{S}]_{k,\ell}$ is the RCS of the ℓth snapshot of the kth target, $\ell = 1, 2, \cdots, L$, with L being the number of snapshots. In this paper, we adopt the Swerling II model and the distribution of the RCS of the kth target is assumed the same for all snapshots, that is, $[\mathbf{S}]_{k,\ell} \sim \mathcal{N}(0, \alpha_k^2)$, $k = 1, 2, \cdots, K$, $\ell = 1, 2, \cdots, L$. The entries of $\mathbf{Q}$ are zero-mean white Gaussian samples and independent of each other, that is, vec($\mathbf{Q}$) $\sim \mathcal{N}(\mathbf{0}_{MNL\times 1}, \sigma^2\mathbf{I}_{MNL})$ where σ^2 is the noise power. The values of $\{\alpha_k^2\}$ and σ^2 are unknown. In the following, we express the DODs and DOAs as spatial frequencies by assigning $\theta_k = 2\pi d_t \sin(\breve{\theta}_k)/\lambda$ and $\phi_k = 2\pi d_r \sin(\breve{\phi}_k)/\lambda$ for brevity. Since d_t, d_r, and λ are known and both $|\breve{\theta}_k|$ and $|\breve{\phi}_k|$ are less than $\pi/2$, our task of estimating the DODs and DOAs is equivalent to finding θ_k and ϕ_k, $k = 1, 2, \cdots, K$.

III. ALGORITHM DEVELOPMENT

The covariance matrix of the received data, denoted by $\mathbf{R}$, can be written as

$$\mathbf{R} = \frac{1}{L}\mathbb{E}\left\{\mathbf{X}\mathbf{X}^H\right\} = \mathbf{F}\mathbf{\Upsilon}\mathbf{F}^H + \sigma^2\mathbf{I}_{MN} \tag{9}$$

where

$$\mathbf{\Upsilon} = \text{diag}\,(\boldsymbol{\upsilon}), \quad \boldsymbol{\upsilon} = \begin{bmatrix}\alpha_1^2 & \alpha_2^2 & \cdots & \alpha_K^2\end{bmatrix}^T \tag{10}$$

If θ_k and ϕ_k are sampled from a distribution that is continuous with respect to the Lebesgue measure in $\mathbb{C}^{2K}$, then the ranks of $\mathbf{F}$ and $\mathbf{R}$ are K almost surely [19]. By using eigenvalue decomposition (EVD), $\mathbf{R}$ is factorized as

$$\begin{aligned}\mathbb{R} = {} & \mathbf{U}_s\,\text{diag}\,([\lambda_1 \quad \lambda_2 \quad \cdots \quad \lambda_K])\,\mathbf{U}_s^H \\ & + \mathbf{U}_n\,\text{diag}\,([\lambda_{K+1} \quad \lambda_{K+2} \quad \cdots \quad \lambda_{MN}])\,\mathbf{U}_n^H\end{aligned} \tag{11}$$

where

$$\lambda_1 \geq \lambda_2 \geq \cdots \geq \lambda_K > \lambda_{K+1} = \cdots = \lambda_{MN} = \sigma^2. \tag{12}$$

Here, $\mathbf{U}_s \in \mathbb{C}^{MN\times K}$ and $\mathbf{U}_n \in \mathbb{C}^{MN\times(MN-K)}$ represent the signal and noise subspaces, respectively. Furthermore,

$\lambda_1, \lambda_2, \cdots, \lambda_{MN}$, are the eigenvalues corresponding to $[\mathbf{U}_s\ \mathbf{U}_n]$. As $\mathbf{U}_s$ spans the same space as $\mathbf{F}$, we have

$$\mathbf{F}\mathbf{T} = \mathbf{U}_s \tag{13}$$

where $\mathbf{T} \in \mathbb{C}^{K\times K}$ is an unknown full-rank matrix. Next, we define an index matrix $\mathcal{I}$ as

$$\mathcal{I} = \begin{bmatrix} 1 & M+1 & \cdots & M(N-1)+1 \\ 2 & M+2 & \cdots & M(N-1)+2 \\ \vdots & \vdots & \ddots & \vdots \\ M & 2M & \cdots & MN \end{bmatrix}. \tag{14}$$

Let $\mathbf{U}_1$ and $\mathbf{U}_2$ be two submatices of $\mathbf{U}_s$ containing the rows indexed by the first and last $(M-1)$ rows of $\mathcal{I}$, respectively. It can be shown that

$$\mathbf{U}_1 = (\mathbf{H} \circ \mathbf{G}_1)\,\mathbf{T} \tag{15}$$

and

$$\mathbf{U}_2 = (\mathbf{H} \circ \mathbf{G}_2)\,\mathbf{T} \tag{16}$$

where $\mathbf{G}_1$ and $\mathbf{G}_2$ contain the first and last $(M-1)$ rows of $\mathbf{G}$, respectively. From (15) and (16), we have

$$\begin{aligned}
&\mathbf{U}_1^{\dagger}\mathbf{U}_2 \\
&= \left(\mathbf{T}^H(\mathbf{H}\circ\mathbf{G}_1)^{\,H}(\mathbf{H}\circ\mathbf{G}_1)\,\mathbf{T}\right)^{-1}\mathbf{T}^H(\mathbf{H}\circ\mathbf{G}_1)^H(\mathbf{H}\circ\mathbf{G}_2)\,\mathbf{T} \\
&= \mathbf{T}^{-1}\left((\mathbf{H}\circ\mathbf{G}_1)^H(\mathbf{H}\circ\mathbf{G}_1)\right)^{-1}(\mathbf{H}\circ\mathbf{G}_1)^H\,(\mathbf{H}\circ\mathbf{G}_2)\,\mathbf{T} \\
&= \mathbf{T}^{-1}\left((\mathbf{H}\circ\mathbf{G}_1)^{\,H}(\mathbf{H}\circ\mathbf{G}_1)\right)^{-1}(\mathbf{H}\circ\mathbf{G}_1)^{\,H}(\mathbf{H}\circ(\mathbf{G}_1\boldsymbol{\Omega}))\,\mathbf{T} \\
&= \mathbf{T}^{-1}\left((\mathbf{H}\circ\mathbf{G}_1)^H\,(\mathbf{H}\circ\mathbf{G}_1)\right)^{-1}(\mathbf{H}\circ\mathbf{G}_1)^{\,H}\,(\mathbf{H}\circ\mathbf{G}_1)\,\boldsymbol{\Omega}\mathbf{T} \\
&= \mathbf{T}^{-1}\boldsymbol{\Omega}\mathbf{T}.
\end{aligned} \tag{17}$$

Note that the third line is obtained from the second line using $\mathbf{G}_2 = \mathbf{G}_1\boldsymbol{\Omega}$ where $\boldsymbol{\Omega} = \mathrm{diag}(\mathbf{a})$ with $\mathbf{a} = [a_1\ a_2 \cdots a_K]^T$ and a_k is defined in (7). Moreover, the fourth line is obtained from the third one using the fact that $\mathbf{H}\circ(\mathbf{G}_1\boldsymbol{\Omega}) = \mathbf{H}\circ(\mathbf{G}_1\circ\mathbf{a}^T) = (\mathbf{H}\circ\mathbf{G}_1)\circ\mathbf{a}^T = (\mathbf{H}\circ\mathbf{G}_1)\boldsymbol{\Omega}$. Similarly, we can construct two matrices, $\mathbf{U}_3 = \mathbf{H}_1\circ\mathbf{G}$ and $\mathbf{U}_4 = \mathbf{H}_2\circ\mathbf{G}$, which are two submatrices of $\mathbf{U}_s$ containing the rows indexed by the first and last $(N-1)$ columns of $\mathcal{I}$, respectively. Here, $\mathbf{H}_1$ and $\mathbf{H}_2$ are $\mathbf{H}$ except with the last and first rows being removed. Following the same procedure, we obtain

$$\mathbf{U}_3^{\dagger}\mathbf{U}_4 = \mathbf{T}^{-1}\boldsymbol{\Gamma}\mathbf{T} \tag{18}$$

where $\boldsymbol{\Gamma} = \mathrm{diag}(\mathbf{b})$ with $\mathbf{b} = [b_1\ b_2 \cdots b_K]^T$ and b_k being defined in (8). In the 2-D ESPRIT algorithm [11], $\mathbf{b}$ and $\mathbf{T}$ are estimated via EVD of (18). Then, $\mathbf{T}$ is substituted back into (17) to obtain $\boldsymbol{\Omega}$ whose diagonal elements are the estimate of $\mathbf{a}$. In practice, $\mathbf{R}$ is replaced by the sample covariance matrix $\hat{\mathbf{R}} = \mathbf{X}\mathbf{X}^H/L$. In this case, (12) is modified as $\hat{\lambda}_1 \geq \hat{\lambda}_2 \geq \cdots \geq \hat{\lambda}_K > \hat{\lambda}_{K+1} \geq \cdots \geq \hat{\lambda}_{MN} > \sigma^2$. Furthermore, $\mathbf{a}$, $\mathbf{b}$, $\mathbf{G}$, $\mathbf{H}$, $\mathbf{U}_s$, $\mathbf{F}$, $\mathbf{T}$, $\boldsymbol{\Omega}$, $\boldsymbol{\Gamma}$ and $\mathbf{U}_i$, $i = 1, 2, 3, 4$, are replaced by their estimated quantities, $\hat{\mathbf{a}}$, $\hat{\mathbf{b}}$, $\hat{\mathbf{G}}$, $\hat{\mathbf{H}}$, $\hat{\mathbf{U}}_s$, $\hat{\mathbf{F}}$, $\hat{\mathbf{T}}$, $\hat{\boldsymbol{\Omega}}$, $\hat{\boldsymbol{\Gamma}}$ and $\hat{\mathbf{U}}_i$, $i = 1, 2, 3, 4$.

Similar to the ESPRIT, the proposed algorithm first applies EVD on $\hat{\mathbf{R}}$ to obtain $\hat{\mathbf{T}}$, then $\hat{\mathbf{F}}$ is estimated as $\hat{\mathbf{F}} = \hat{\mathbf{U}}_s\hat{\mathbf{T}}^{-1}$. Analogous to $\hat{\mathbf{U}}_i$, we define $\hat{\mathbf{F}}_i$, $i = 1, 2, 3, 4$. The $\hat{\mathbf{b}}$ is obtained as the diagonal elements of $\hat{\boldsymbol{\Gamma}}$ which is computed from

$$\hat{\boldsymbol{\Gamma}} = \hat{\mathbf{F}}_3^{\dagger}\hat{\mathbf{F}}_4. \tag{19}$$

In a similar manner, $\mathbf{a}$ is estimated from the diagonal elements of $\hat{\boldsymbol{\Omega}}$:

$$\hat{\boldsymbol{\Omega}} = \hat{\mathbf{F}}_1^{\dagger}\hat{\mathbf{F}}_2. \tag{20}$$

In the existing DOD and DOA estimation algorithms [11–13], $\mathbf{a}$ and $\mathbf{b}$ are calculated using (20) and (19) with some modifications, respectively, and the whole algorithm terminates. Unlike these algorithms, we continuously update $\hat{\mathbf{a}}$ and $\hat{\mathbf{F}}$. The details of our proposed iterative algorithm are given as follows. First, note that from (13), we have

$$\mathbf{F} = \mathbf{U}_s\mathbf{T}^{-1} \tag{21}$$

and

$$\mathbf{T}^{-1} = \mathbf{U}_s^{\dagger}\mathbf{F}. \tag{22}$$

Combining (21) and (22) yields

$$\mathbf{F} = \mathbf{U}_s\mathbf{U}_s^{\dagger}\mathbf{F}. \tag{23}$$

In reality, $\mathbf{F}$ and $\mathbf{U}_s$ are replaced by $\hat{\mathbf{F}}$ and $\hat{\mathbf{U}}_s$, respectively, and (23) provides an update of $\hat{\mathbf{F}}$. Note that $\hat{\mathbf{F}}$ on the right hand side of (23) is constructed using $\hat{\mathbf{G}}$ and $\hat{\mathbf{H}}$ in (2) with $\hat{\mathbf{a}}$ and $\hat{\mathbf{b}}$, obtained from (20) and (19), respectively. After calculating a new $\hat{\mathbf{F}}$, we reestimate $\hat{\boldsymbol{\Omega}}$ and $\hat{\mathbf{a}}$ using (20). To ensure that the newly computed $\hat{\mathbf{a}}$ and $\hat{\mathbf{b}}$ are sufficiently accurate, we adopt a checking condition as follows. First, vectorizing both sides of (9) yields

$$\mathbf{r} = \left(\mathbf{F}^*\circ\mathbf{F}\right)\boldsymbol{\upsilon} + \sigma^2\boldsymbol{i} \tag{24}$$

where $\mathbf{r} = \mathrm{vec}(\mathbf{R})$ and $\boldsymbol{i} = \mathrm{vec}(\mathbf{I}_{MN})$. Rewriting (24) in a more compact manner, we have

$$\mathbf{r} = \boldsymbol{\mathcal{F}}\boldsymbol{\zeta} \tag{25}$$

where $\boldsymbol{\mathcal{F}} = [\mathbf{F}^*\circ\mathbf{F}\ \ \boldsymbol{i}]$ and $\boldsymbol{\zeta} = [\boldsymbol{\upsilon}^T\ \ \sigma^2]^T$. Substituting $\boldsymbol{\zeta} = \boldsymbol{\mathcal{F}}^{\dagger}\mathbf{r}$ into (25) yields

$$\mathbf{P}_{\boldsymbol{\mathcal{F}}}^{\perp}\mathbf{r} = \mathbf{0}_{M^2N^2\times 1} \tag{26}$$

where $\mathbf{P}_{\boldsymbol{\mathcal{F}}}^{\perp}\mathbf{r} = (\boldsymbol{\mathcal{F}}\boldsymbol{\mathcal{F}}^{\dagger} - \mathbf{I}_{M^2N^2})$. Therefore, when a new $\hat{\mathbf{F}}$ is calculated, we also get $|\mathbf{P}_{\hat{\boldsymbol{\mathcal{F}}}}^{\perp}\mathbf{r}|$ according to (26). Upon convergence of $\hat{\mathbf{F}}$, the parameter vector $\hat{\mathbf{a}}$ with minimum value of (26) will be the final solution. We see that pairing of DODs and DOAs is automatically achieved. The proposed algorithm is summarized in algorithm 1. It is novel in the sense that it utilizes an iterative update procedure and includes an accuracy checkup step to ensure that the DOD and DOA estimates are always more accurate than the initial estimate. Therefore, the proposed algorithm is expected to outperform the existing ones. We show later in Section V that the proposed algorithm can provide higher estimation accuracy, especially in the scenario of identical DODs or DOAs. The main computation of the proposed algorithm consists of two parts. First, construction of $\mathbf{R}$ requires $O(M^2N^2L)$, which

is also required in the 2-D ESPRIT and ESPRIT algorithms. The second part is the calculation of $\mathbf{P}_{\hat{\mathcal{F}}}^{\perp}$, whose complexity is $O(M^6N^6)$. When L is large compared with MN, its complexity is comparable to that of the existing ESPRIT algorithms. However, note that when $M < N$ and $K = MN - M$, the 2-D ESPRIT algorithm fails to operate because $\mathbf{U}_1, \mathbf{U}_2 \in \mathbb{C}^{(MN-N)\times K}$ are fat matrices and thus $\boldsymbol{\Omega}$ cannot be calculated. However, the proposed and ESPRIT algorithms first calculate $\boldsymbol{\Gamma}$ and then construct $\mathbf{F}$ to estimate $\boldsymbol{\Omega}$. Therefore, both $\mathbf{a}$ and $\mathbf{b}$ can be estimated. As $\mathbf{U}_3$ and $\mathbf{U}_4$ have dimensions $(MN - M) \times K$, K is at most $(MN - M)$ to produce a unique $\boldsymbol{\Gamma}$. Consequently, the number of identifiable targets of the proposed algorithm is up to $(MN - M)$. However, this number is the upper bound and in some situations, the proposed algorithm fails to work when there are $(MN - M)$ targets. For example, when $K = N = M + 1$ and all of the DOAs are the same, that is, $\mathbf{b} = b\mathbf{1}_K$ and $\mathbf{H}_1 = \boldsymbol{h}\mathbf{1}_K^T$ where $\boldsymbol{h} \in \mathbb{C}^{N-1}$ is the vector containing the first $(N - 1)$ elements of $\mathbf{h}_1$ in (6). Then, $\mathbf{F} = \mathbf{H} \circ \mathbf{G} = \boldsymbol{h}\mathbf{1}_K{}^T \circ \mathbf{G} = (\boldsymbol{h} \otimes \mathbf{I}_M)(\mathbf{1}_K^T \circ \mathbf{G}) = (\boldsymbol{h} \otimes \mathbf{I}_M)\mathbf{G}$. As the dimensions of the first and second matrices are $MN \times M$ and $M \times K$, respectively, the rank of $\mathbf{F}$ is $M < K$. As a result, $\mathbf{U}_s$ cannot be obtained and the proposed algorithm fails to work. Another example is the scenario of $N = M + 1$, $K = 2M$, and DODs and DOAs are uniformly spaced with same offset δ. Mathematically, $\mathbf{G} = [\mathbf{g}_1 \ \boldsymbol{\Delta}\mathbf{g}_1 \ \cdots \ \boldsymbol{\Delta}^{K-1}\mathbf{g}_1]$, $\mathbf{H}_1 = [\boldsymbol{h} \ \boldsymbol{\Delta}\boldsymbol{h} \ \cdots \ \boldsymbol{\Delta}^{K-1}\boldsymbol{h}]$, $\boldsymbol{\Delta} = \text{diag}(\boldsymbol{\delta})$ and $\boldsymbol{\delta} = [1 \ \delta \ \cdots \ \delta^{M-1}]^T$ is a steering vector with $|\boldsymbol{\delta}| = 1$. Then, $\mathbf{H}_1 \circ \mathbf{G} = [\widetilde{\boldsymbol{f}} \ (\boldsymbol{\Delta} \otimes \boldsymbol{\Delta})\widetilde{\boldsymbol{f}} \ \cdots \ (\boldsymbol{\Delta} \otimes \boldsymbol{\Delta})^{K-1}\widetilde{\boldsymbol{f}}] = [\widetilde{\mathbf{F}}\mathbf{1}_{M^2} \ \widetilde{\mathbf{F}}(\boldsymbol{\delta} \otimes \boldsymbol{\delta}) \ \cdots \ \widetilde{\mathbf{F}}(\boldsymbol{\delta} \otimes \boldsymbol{\delta}) \odot (\boldsymbol{\delta} \otimes \boldsymbol{\delta}) \cdots \odot (\boldsymbol{\delta} \otimes \boldsymbol{\delta})] = \widetilde{\mathbf{F}}\widetilde{\boldsymbol{\Delta}}$ where $\widetilde{\boldsymbol{f}} = \boldsymbol{h} \otimes \mathbf{g}_1$, $\widetilde{\mathbf{F}} = \text{diag}(\widetilde{\boldsymbol{f}})$, $\widetilde{\boldsymbol{\Delta}} = [\mathbf{1}_{M^2} \ (\boldsymbol{\delta} \otimes \boldsymbol{\delta}) \ \cdots \ (\boldsymbol{\delta} \otimes \boldsymbol{\delta}) \odot (\boldsymbol{\delta} \otimes \boldsymbol{\delta}) \cdots \odot (\boldsymbol{\delta} \otimes \boldsymbol{\delta})]$. Note that $\boldsymbol{\delta} \otimes \boldsymbol{\delta} \in \mathbb{C}^{M^2}$ equals $\text{vec}(\boldsymbol{\delta}\boldsymbol{\delta}^T)$. As $\boldsymbol{\delta} \in \mathbb{C}^M$ is a steering vector, $\boldsymbol{\delta}\boldsymbol{\delta}^T \in \mathbb{C}^{M\times M}$ is a Hermitian Toeplitz matrix. Hence, there are $(2M - 1)$ distinct elements in $\boldsymbol{\delta}\boldsymbol{\delta}^T$ and $\boldsymbol{\delta} \otimes \boldsymbol{\delta}$ as well as all the columns of $\tilde{\boldsymbol{\Delta}}$. Now, the ranks of $\widetilde{\mathbf{F}}$ and $\tilde{\boldsymbol{\Delta}}$ are M^2 and $(2M - 1)$, respectively, and it implies that the rank of $(\mathbf{H}_1 \circ \mathbf{G})$ is $(2M - 1) < 2M = K$. As a result, $\boldsymbol{\Gamma}$ cannot be estimated and the proposed algorithm fails.

IV. IDENTIFIABILITY OF MUSIC

We will prove that when $K = MN - 1$, the MUSIC algorithm fails to operate even when there are infinite snapshots, that is, $L \to \infty$. In this case, $\hat{\mathbf{R}} = \mathbf{R}$ defined in (9). In the MUSIC algorithm, the noise subspace which is a vector, denoted by $\mathbf{u} \in \mathbb{C}^{MN}$, is first computed. Then, θ_k and ϕ_k, $k = 1, 2, \cdots, K$, are found by solving $\|\mathbf{F}^H\mathbf{u}\|^2 = 0$. However, it will be shown that when $K = MN - 1$, there are more than K sets of (θ_k, ϕ_k) solutions, indicating the nonidentifiability of parameters. First, we have

$$\mathbf{F}^H\mathbf{u} = \mathbf{0}_{K\times 1}. \tag{27}$$

Next, we show that $\mathbf{u}$ equals the conjugate of its reversal.

LEMMA 1

$$\mathbf{J}_{MN}\mathbf{u} = \mathbf{u}^* \tag{28}$$

Algorithm 1 Iterative ESPRIT Algorithm

Require: $\mathbf{X}$, M, N, K, tolerance ϵ, maximum number of iterations D
Initialization: $i \leftarrow 0$, $d \leftarrow \infty$
Compute $\hat{\mathbf{R}} = \frac{1}{L}\mathbf{X}\mathbf{X}^H$.
Compute K dominant singular vectors of $\hat{\mathbf{R}}$, $\hat{\mathbf{U}}_s$ and submatrices $\hat{\mathbf{U}}_i$, $i = 1, 2, 3, 4$
Compute eigenvalues and eigenvectors of $\hat{\mathbf{U}}_3^{\dagger}\hat{\mathbf{U}}_4$, denoted by $\hat{\mathbf{b}}$ and $\hat{\mathbf{T}}$
Compute $\hat{\mathbf{F}} = \hat{\mathbf{U}}_s\hat{\mathbf{T}}^{-1}$
Compute $\hat{\boldsymbol{\Gamma}} = \hat{\mathbf{F}}_3^{\dagger}\hat{\mathbf{F}}_4$
Compute $\hat{\mathbf{b}}$ and $\hat{\mathbf{H}}$
while $i \epsilon$ and $d > D$ do
  Set $\hat{\mathbf{F}}_{\text{old}} = \hat{\mathbf{F}}$
  Compute $\hat{\mathbf{a}} = \text{diag}(\hat{\mathbf{F}}_1^{\dagger}\hat{\mathbf{F}}_2)$
  Compute $\hat{\mathbf{G}}$ and $\hat{\mathbf{F}}$
  Compute $\hat{\mathbf{F}} = \hat{\mathbf{U}}_s\hat{\mathbf{U}}_s^{\dagger}\hat{\mathbf{F}}$
  Compute $d = |\hat{\mathbf{F}} - \hat{\mathbf{F}}_{\text{old}}|$
  Compute $\mathbf{e}_i = |\mathbf{P}_{\hat{\mathcal{F}}}^{\perp}\mathbf{r}|$
  $\hat{\mathbf{a}}_i \leftarrow \hat{\mathbf{a}}$
  $i \leftarrow i + 1$
end while
$\hat{\mathbf{a}} = \hat{\mathbf{a}}_k$ where $\mathbf{e}_k < \mathbf{e}_j$, $j = 1, 2, \cdots, P$, $j \neq k$ and P is the number of elements in $\mathbf{e}$
return $\hat{\mathbf{a}}$ and $\hat{\mathbf{b}}$

where $\mathbf{J}_{MN} \in \mathbb{R}^{MN\times MN}$ is the exchange matrix with all elements being zero except one in the antidiagonal.

PROOF Postmultiplying (9) by $\mathbf{u}$ and using (27), we obtain

$$\mathbf{R}\mathbf{u} = \sigma^2\mathbf{u} \tag{29}$$

Employing the idea of forward-backward approach for spatially smoothing, we have $\mathbf{R} = \mathbf{J}_{MN}\mathbf{R}^*\mathbf{J}_{MN}$ and

$$\mathbf{J}_{MN}\mathbf{R}^*\mathbf{J}_{MN}\mathbf{u} = \sigma^2\mathbf{u}. \tag{30}$$

Premultiplying both sides of (30) by $\mathbf{J}_{MN}$ and using $\mathbf{J}_{MN}^2 = \mathbf{I}_{MN}$ yields

$$\mathbf{R}^*\mathbf{J}_{MN}\mathbf{u} = \sigma^2\mathbf{J}_{MN}\mathbf{u}. \tag{31}$$

On the other hand, taking conjugate on both sides of (29), we obtain

$$\mathbf{R}^*\mathbf{u}^* = \sigma^2\mathbf{u}^*. \tag{32}$$

As the rank of $\mathbf{R} \in \mathbb{C}^{(MN)\times(MN)}$ is $K = (MN - 1)$, the eigenvalue σ^2 has multiplicity one. Hence, $\mathbf{u}^*$ is a unique eigenvector corresponding to the eigenvalue σ^2 for $\mathbf{R}^*$. Comparing (31) and (32) yields

$$\mathbf{J}_{MN}\mathbf{u} = \mathbf{u}^*. \tag{33}$$

■

Now, we define the bivariate polynomial $p(y, z)$ as

$$p(y, z) = \mathbf{y}^T\mathbf{U}^*\mathbf{z} \tag{34}$$

where $\mathbf{y} = [1 \ y \ \cdots \ y^{M-1}]^T$, $\mathbf{z} = [1 \ z \ \cdots \ z^{N-1}]^T$, $\mathbf{U}^* = \text{vec}^{-1}(\mathbf{u}^*) \in \mathbb{C}^{M\times N}$. A special type of polynomial called conjugate reciprocal (CR) polynomial is then defined as follows.

DEFINITION A polynomial $f(x) = \sum_{m=0}^{M} a_m x^m$ is CR if $a_m = a_{M-m}^*$.

Let $y_m = \exp(j\theta_m)$, $m = 1, 2, \cdots, M$, and $z_n = \exp(j\phi_n)$, $n = 1, 2, \cdots, N$. Then, we have Lemma 2.

LEMMA 2 The univariate polynomials $p(y, z_n)$, $n = 1, 2, \cdots, N$, and $p(y_m, z)$, $m = 1, 2, \cdots, M$, with degrees $(M-1)$ and $(N-1)$, respectively, are CR up to a proportional constant.

PROOF Lemma 1 implies

$$(\mathbf{J}_N \otimes \mathbf{J}_M)\,\mathbf{u} = \mathbf{u}^*. \tag{35}$$

Using the identity $(\mathbf{ABC}) = (\mathbf{C}^T \otimes \mathbf{A})\text{vec}(\mathbf{B})$, unvectorizing both sides of (35) yields

$$\mathbf{U}^* = \mathbf{J}_M \mathbf{U} \mathbf{J}_N. \tag{36}$$

Postmultiplying both sides of (36) by $\mathbf{h}_n$, we obtain

$$\boldsymbol{h}_n \triangleq \mathbf{U}^*\mathbf{h}_n = \mathbf{J}_M \mathbf{U} \mathbf{J}_N \mathbf{h}_n = z_n^{N-1}\left(\mathbf{J}_M \mathbf{U} \mathbf{h}_n^*\right). \tag{37}$$

where the relationship $\mathbf{J}_N \mathbf{h}_n = \mathbf{h}_n^* z_n^{N-1}$ is used. As $\boldsymbol{h}_n \propto \mathbf{J}_M \boldsymbol{h}_n^*$, the polynomial $p(y, z_n) = \mathbf{y}^T \boldsymbol{h}_n$ is CR up to the proportional constant z_n^{N-1}. Similarly, we can show that $\boldsymbol{g}_m^T \triangleq \mathbf{g}_m^T \mathbf{U}^* = y_m^{M-1} \mathbf{g}_m^H \mathbf{U} \mathbf{J}_N$. Hence, $f(y_m, z) = \boldsymbol{g}_m^T \mathbf{z}$ is CR up to the proportional constant y_n^{M-1}. ■

THEOREM 1 The roots of the CR polynomial equation are either

1) unimodular, that is, they lie on the unit circle in the complex plane
2) appear in CR pair, that is, if a is a root, then so is $1/a^*$. ■

PROOF See [20].

Finally, we come to the most important result.

THEOREM 2 When $L \to \infty$ and $K = MN - 1$, there exists the $(K+1)$th set of solution, namely, $(\theta_{K+1}, \phi_{K+1}) \neq (\theta_k, \phi_k)$, $k = 1, 2, \cdots, K$, satisfying $(\mathbf{h}_{K+1} \otimes \mathbf{g}_{K+1})^H \mathbf{u} = 0$ where $\mathbf{g}_{K+1} = [1 \;\; \exp(j\theta_{K+1}) \;\; \cdots \;\; \exp(j(M-1)\theta_{K+1})]^T$ and $\mathbf{h}_{K+1} = [1 \;\; \exp(j\phi_{K+1}) \;\; \cdots \;\; \exp(j(N-1)\phi_{K+1})]^T$.

PROOF To prove the existence of the $(K+1)$th DOD and DOA, we consider two cases:

1) M and N are not all odd
2) both M and N are odd.

In the first case, either M or N is even. Without loss of generality, let N be even. Assign $\theta_{K+1} \neq \theta_k$, $k = 1, 2, \cdots, K$. Then, we are going to show that at least one of the roots of the CR polynomial equation $p(\exp(j\theta_{K+1}), z) = 0$, with the proportional constant being removed, is unimodular. Note that the degree of $p(\exp(j\theta_{K+1}), z)$ is $(N-1)$, which is odd, and thus $p(\exp(j\theta_{K+1}), z) = 0$ has an odd number of roots. By Theorem 1, there are at most $(N-2)/2$ pairs of nonunimodular roots and thus at least one root is unimodular, namely, ϕ_{K+1}. Therefore, we have $p(\exp(j\theta_{K+1}), \exp(j\phi_{K+1})) = 0$, $\theta_{K+1} \neq \theta_k$, $k = 1, 2, \cdots, K$, and the nonidentifiability is proved.

In the second case, without loss of generality, we consider $p(\exp(j\theta_k), z) = 0$, $k = 1, 2, \cdots, K$, whose degrees are all even. Apart from $\exp(j\phi_k)$, $k = 1, 2, \cdots, K$, all the K polynomial equations have odd numbers of roots. Similar to the first case, there exists at least one unimodular root for $p(\exp(j\theta_k), z) = 0$, $k = 1, 2, \cdots, K$, namely, $z_k = \exp(j\tilde{\phi}_k)$. It remains to show that $\tilde{\phi}_k \neq \phi_k$ for all k. Suppose on the contrary, $\tilde{\phi}_k = \phi_k$, $k = 1, 2, \cdots, K$, that is, all the polynomial equations $p(\exp(j\theta_k), z) = 0$ have repeated roots. Then, we have $p'(\exp(j\theta_k), \exp(j\phi_k)) = 0$ where $p'(y, z)$ denotes $dp(y, z)/(dz)$, $k = 1, 2, \cdots, K$. Expressing it in matrix form yields

$$\mathbf{g}_k^T \mathbf{V}^* \mathbf{h}_k = 0, \quad k = 1, 2, \cdots, K \tag{38}$$

where

$$\mathbf{V}^* = \mathbf{U}^* \text{diag}\left([0 \;\; 1 \;\; \cdots \;\; N-1]\right). \tag{39}$$

Vectorizing and grouping all vectors yields

$$\mathbf{v}^H \mathbf{F} = \mathbf{0}_{1\times K} \tag{40}$$

where $\mathbf{v} = \text{vec}(\mathbf{V})$. On the other hand, substituting $\mathbf{y} = \mathbf{g}_k$ and $\mathbf{z} = \mathbf{h}_k$ into (34) and performing similar operations, we get

$$\mathbf{u}^H \mathbf{F} = \mathbf{0}_{1\times K}. \tag{41}$$

Combining (32) and (33) yields

$$\begin{bmatrix}\mathbf{u} & \mathbf{v}\end{bmatrix}^H \mathbf{F} = \mathbf{0}_{2\times K}. \tag{42}$$

As $\mathbf{u}$ and $\mathbf{v}$ are linearly independent, the first matrix on the left hand side has rank 2. Nevertheless, the dimension of the left null space of the full rank matrix $\mathbf{F} \in \mathbb{C}^{MN\times K}$ where $K = MN - 1$, is only one. It leads to a contradiction and hence $\tilde{\phi}_k \neq \phi_k$ for all k, which results in nonidentifiability. ■

REMARK Recall that the identifiability limit of the ESPRIT algorithm is lower than that of the MUSIC method because the latter fully utilizes the noise subspace. As a result, the former cannot identify $(MN-1)$ targets as well. This also aligns with our analysis in Section III.

V. SIMULATION RESULTS

Computer simulations are carried out to evaluate the performance of the proposed algorithm by comparing with the 2-D ESPRIT [11], ESPRIT [12], Chen et al.'s [13] algorithms, reduced-dimension (RD)-MUSIC approach [21], as well as ML algorithm [14] for joint DOD and DOA estimation in bistatic MIMO radar. Furthermore, the results of the MUSIC approach [17] initialized by [11–13], are included, while the Cramér-Rao bound (CRB) is employed as the performance benchmark [12]. The tolerance ϵ is set to 10^{-6} and the maximum number of iterations is assigned as $D = 10$. The mean square error (MSE) is employed as the performance measure:

$$\text{MSE}\,(\boldsymbol{\theta}) = \frac{1}{KR}\sum_{r=1}^{R}\sum_{k=1}^{K}\left(\theta_k - \hat{\theta}_{k,r}\right)^2 \tag{43}$$

TABLE I
θ_k and ϕ_k in First Test

	DOD//DOA	
k	θ_k/π	ϕ_k/π
1	−0.81	−0.78
2	−0.74	−0.48

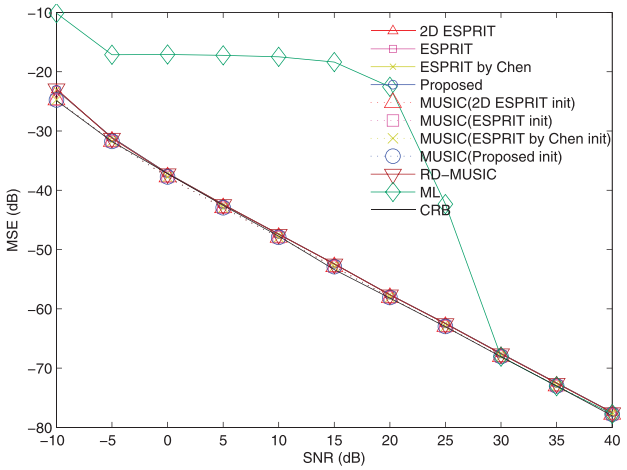

Fig. 1. MSE of $\hat{\theta}_k$ versus SNR at $K = 2$ and $L = 256$.

$$\text{MSE}(\phi) = \frac{1}{KR}\sum_{r=1}^{R}\sum_{k=1}^{K}\left(\phi_k - \hat{\phi}_{k,r}\right)^2 \qquad (44)$$

where $R = 1000$ is the number of independent runs, and $\hat{\theta}_{k,r}$ and $\hat{\phi}_{k,r}$ are the estimates of θ_k and ϕ_k in the rth trial. We properly scale the noise matrix $\mathbf{Q}$ whose entries are circular complex-valued zero-mean white Gaussian variables, to produce different signal-to-noise ratio (SNR) conditions. The SNR is defined as $\sum_{m=1}^{MN}\sum_{\ell=1}^{L}\|\mathbf{F}^H\boldsymbol{\Upsilon}\mathbf{F}\|^2/(\sigma^2 MNL)$.

In the first test, overdetermined parameter estimation is investigated. The parameter settings are $M = 4$, $N = 5$, $d_t = d_r = 0.25$, $K = 2$, $L = 256$ while the DODs and DOAs are listed in Table I. From Figs. 1 and 2, it is seen that the MSE difference between the proposed and other ESPRIT-type algorithms is negligible when SNR $\geq$ –5 dB except that the ML algorithm has a larger threshold SNR, which is 30 dB because of inaccurate initialization. Furthermore, the MSEs of all ESPRIT algorithms are very close to the CRB. We also see that the MUSIC algorithm provides similar performance with different initializations. As the number of targets is small compared with M and N, the accuracy of all methods is very high. The average computational times of the proposed approach [11–14, 21] for a single run are 1.80×10^{-3} s, 7.55×10^{-4} s, 5.44×10^{-4} s, 5.20×10^{-4} s, 8.22×10^{-1} s, and 47.95 s, respectively.

In the second test, we study the performance of the proposed algorithm in underdetermined DOD and DOA estimation. The parameters are the same as before except that $K = 8$ and the additional $\{\theta_k\}$ and $\{\phi_k\}$ are shown in

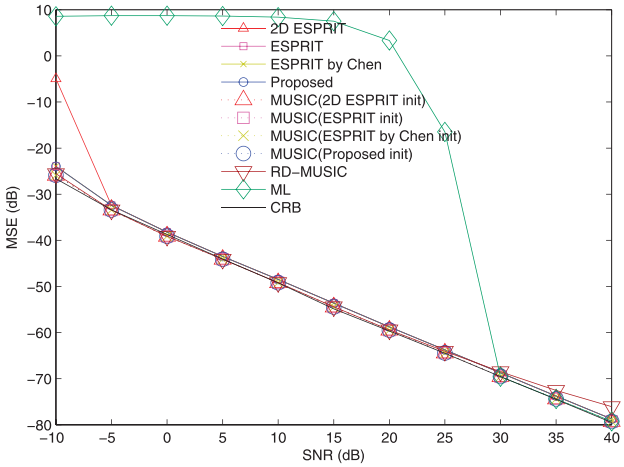

Fig. 2. MSE of $\hat{\phi}_k$ versus SNR at $K = 2$ and $L = 256$.

TABLE II
Additional θ_k and ϕ_k in Second and Third Tests

	DOD//DOA	
k	θ_k/π	ϕ_k/π
3	−0.72	−0.07
4	−0.66	0.76
5	−0.61	0.55
6	−0.52	−0.75
7	−0.38	0.89
8	−0.22	−0.88

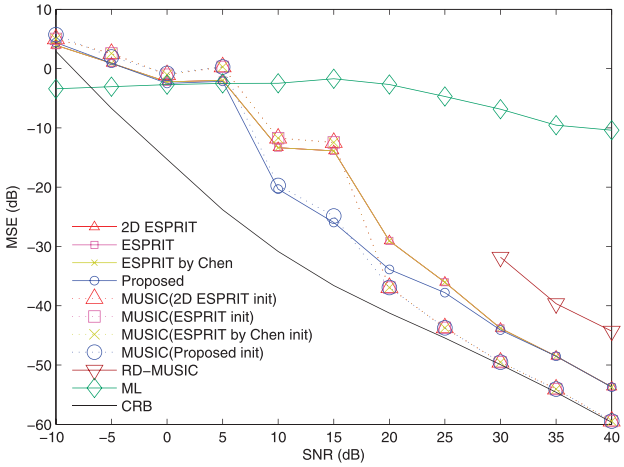

Fig. 3. MSE of $\hat{\theta}_k$ versus SNR at $K = 8$ and $L = 256$.

Table II. From Figs. 3 and 4, it is observed that the threshold SNR of the algorithms in [11–13] are 20 dB while that of the proposed algorithm is 10 dB. The ML algorithm [14] performs unsatisfactorily because of poor initialization while the algorithm in [21] is even worse as it cannot resolve K pairs of DODs/DOAs for SNR $<$ 30 dB. The superiority of our proposal in terms of estimation performance over the other algorithms is demonstrated in this more challenging environment. Furthermore, the MUSIC algorithm performs similarly with different initializations when SNR $\geq$ 20 dB. The

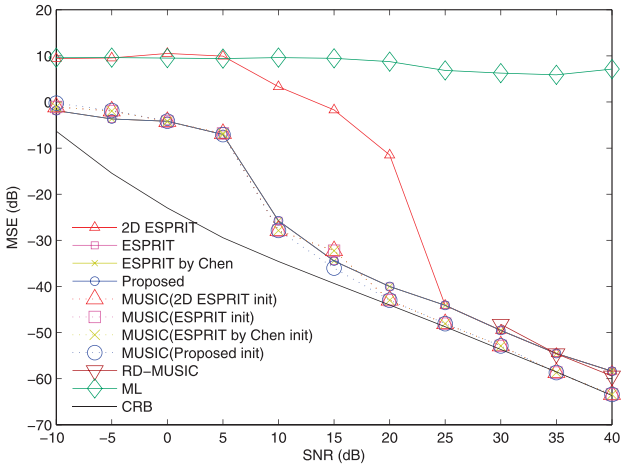

Fig. 4. MSE of $\hat{\phi}_k$ versus SNR at $K = 8$ and $L = 256$.

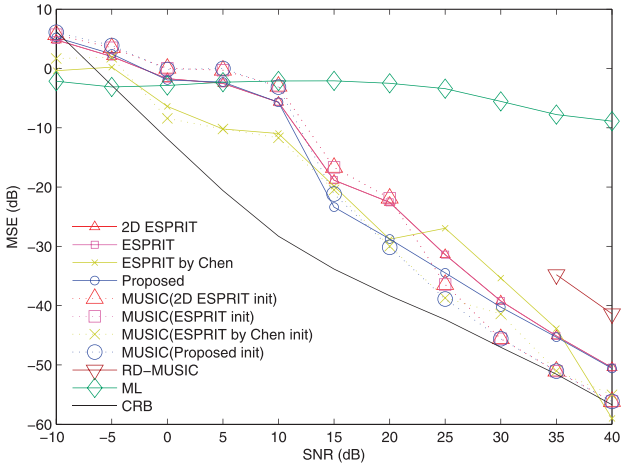

Fig. 5. MSE of $\hat{\theta}_k$ versus SNR at $K = 8$ and $L = 128$.

average computational times of the proposed algorithm [11–14, 21] for a single run are 9.80×10^{-3} s, 1.42×10^{-3} s, 1.26×10^{-3} s, 1.08×10^{-3} s, 5.54×10^{-1} s, and 70.32 s, respectively.

In the third test, we change the number of snapshots from $L = 256$ to $L = 128$ while keeping the parameters in the second test unchanged. In Fig. 5, the MSE of the proposed algorithm is lower than those of the ESPRIT algorithms when 15 dB $\leq$ SNR $\leq$ 30 dB. The average computational times of the proposed method [11–14, 21] for a single run are 6.97×10^{-3} s, 7.87×10^{-4} s, 8.57×10^{-4} s, 6.29×10^{-4} s, 7.62×10^{-1} s, and 48.28 s, respectively. Similar to previous test, [21] cannot resolve K pairs of DODs/DOAs for SNR $\leq$ 30dB. Furthermore, the MUSIC algorithm can provide nearly optimal estimates using different initializations.

Finally, we investigate the performance of the proposed algorithm in underdetermined situation with identical DODs and DOAs. The parameter settings are the same as in the second test except that K is now set to 10 instead of 8. The additional values of DODs and DOAs are depicted in Table III. Note that there are three identical

TABLE III
Additional θ_k and ϕ_k in Fourth Test

	DOD//DOA	
k	θ_k/π	ϕ_k/π
9	−0.22	−0.48
10	−0.22	−0.78

TABLE IV
Additional θ_k and ϕ_k in Identifiability Test of MUSIC

	DOD//DOA	
k	θ_k/π	ϕ_k/π
11	0.2700	0.06
12	0.32	0.42
13	0.34	0.70
14	0.38	−0.14
15	0.54	0.56
16	0.06	0.22
17	0.80	0.60
18	0.83	0.39
19	0.95	0.11

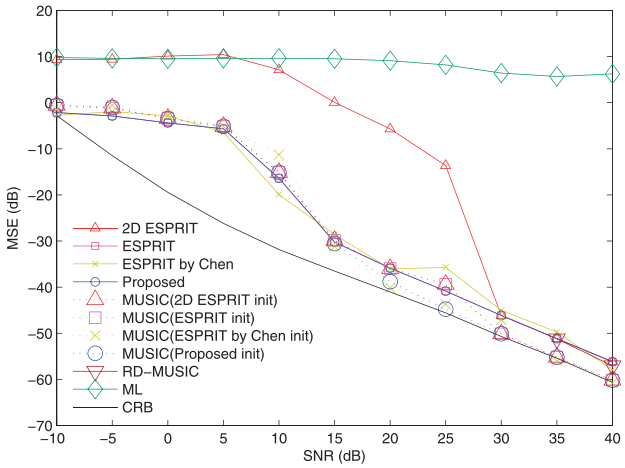

Fig. 6. MSE of $\hat{\phi}_k$ versus SNR at $K = 8$ and $L = 128$.

DODs and two pairs of identical DOAs now. From Figs. 7 and 8, the MSEs of the ESPRIT algorithms remain nearly constant when SNR$\geq$ 15 dB. It implies that they cannot provide accurate DOD and DOA estimates. On the other hand, the proposed algorithm, though suboptimal, is able to provide consistent parameter estimates. In this test, the MUSIC algorithm initialized by the proposed algorithm, can provide nearly optimal estimates when SNR $\geq$ 30 dB while the MUSIC estimates initialized by the ESPRIT algorithms are very poor. That is to say, the MUSIC actually degrades the initial estimate in this case while it improves the estimates for other cases in Figs. 1 to 6. The reason is that in the fourth test, the initial guesses produced by conventional ESPRIT algorithms deviate a lot from the true value. Thus, the parameter estimates provided by the MUSIC algorithm using these poor initializations may be aggravated. On the other hand, in

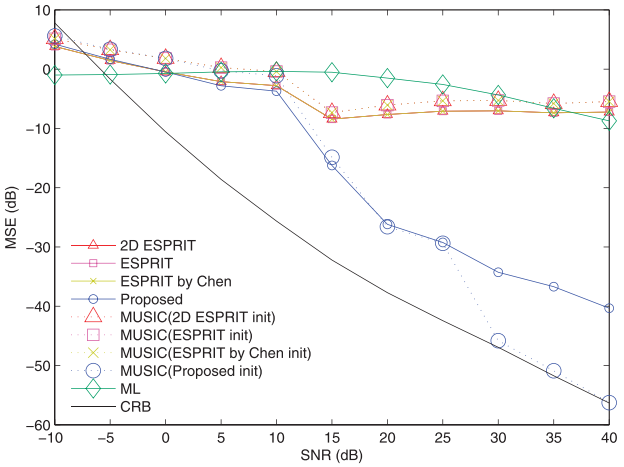

Fig. 7. MSE of $\hat{\theta}_k$ versus SNR for identical DODs and DOAs.

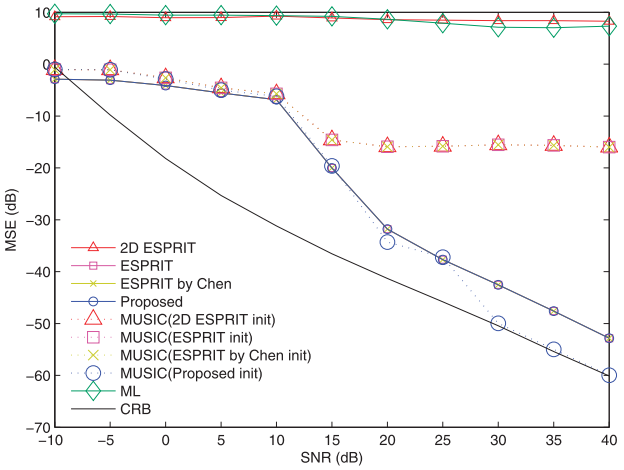

Fig. 8. MSE of $\hat{\phi}_k$ versus SNR for identical DODs and DOAs.

Figs. 1 to 6, the conventional ESPRIT algorithms can produce suboptimal but consistent parameter estimates and the MUSIC algorithm can refine these parameter estimates. As a result, the global optimum of the MUSIC cost function is achieved in Figs. 1 to 6 but not Figs. 7 to 8. This test demonstrates the superiority of the proposed algorithm against the conventional ESPRIT algorithms in very challenging scenarios. Similar to previous scenarios, the algorithm proposed in [21] cannot resolve K pairs of DODs/DOAs for the whole SNR range. The average computational times of the proposed algorithm [11–14] for a single run are 9.56×10^{-3} s, 9.66×10^{-4} s, 9.47×10^{-4} s, 9.44×10^{-4} s, and 48.96 s, respectively.

In summary, the threshold SNR of the DOD/DOA estimated by the proposed algorithm is lower than that of the ESPRIT algorithms. Moreover, the performance of the MUSIC algorithm initialized by the proposed algorithm is also superior to that initialized by the other algorithms and is able to attain nearly optimal performance. Furthermore, the RD-MUSIC approach cannot resolve K peaks when the SNR is low and the performance of the ML algorithm is very sensitive to the initial guess, especially when K is large. On the other hand, the computational complexity of the proposed algorithm is higher than that of the ESPRIT algorithms but lower than that of the ML algorithm.

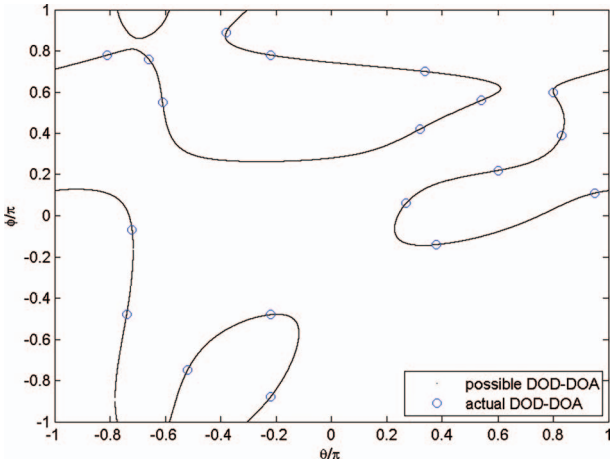

Fig. 9. Nonidentifiability illustration of MUSIC at $K = MN - 1$.

Apart from evaluating the performance of the proposed algorithm, the nonidentifiability of the MUSIC algorithm is illustrated with a numerical example. The parameter settings are the same in the final test except that K is now set to 19 and the extra parameters are shown in Table IV In Fig. 9, we plot the DOD-DOA pairs satisfying (27). We observe that there are infinite solutions. As a result, DODs and DOAs cannot be uniquely identified by the MUSIC algorithm.

VI. CONCLUSION

An iterative ESPRIT algorithm is devised for joint DOD and DOA estimation in the presence of white Gaussian noise for bistatic MIMO radar. The proposed scheme, which includes a parameter-checking procedure, outperforms the conventional ESPRIT approach in challenging scenarios of underdetermined estimation and/or identical DODs and DOAs. Employing its estimates as initial guesses, the MUSIC estimator is able to achieve near-optimal estimation performance at sufficient high SNR conditions. Furthermore, it is proved that the MUSIC algorithm fails to work when the target number is $K = MN - 1$, which is its identifiability limit claimed in the literature.

REFERENCES

[1] Li, J., and Stoica, P.
MIMO radar with colocated antennas: Review of some recent work.
IEEE Signal Processing Magazine, **24**, 5 (2007), 106–114.

[2] Haimovich, A. H., Blum, R. S., and Cimini, L. J.
MIMO radar with widely separated antennas.
IEEE Signal Processing Magazine, **25**, 1 (2008), 116–129.

[3] Li, J., and Stoica, P.
MIMO Radar Signal Processing. New York: Wiley, 2008.

[4] Bekkerman, I., and Tabrikian, J.
Target detection and localization using MIMO radars and sonars.

IEEE Transactions on Signal Processing, **54**, 10 (2006), 3873–3883.

[5] He, Q., Blum, R., and Haimovich, A.
Noncoherent MIMO radar for location and velocity estimation: More antennas means better performance.
IEEE Transactions on Signal Processing, **58**, 7 (2010), 3661–3680.

[6] He, Q., and Blum, R.
Diversity gain for MIMO Neyman-Pearson signal detection.
IEEE Transactions on Signal Processing, **59**, 3 (2011), 869–881.

[7] Hassanien, A., Vorobyov, S. A., and Gershman, A. B.
Moving target parameters estimation in noncoherent MIMO radar systems.
IEEE Transactions on Signal Processing, **60**, 5 (May 2012), 2354–2361.

[8] Stoica, P., Li, J., and Xie, Y.
On probing signal design for MIMO radar.
IEEE Transactions on Signal Processing, **55**, 8 (2007), 4151–4161.

[9] Chen, C. Y., and Vaidyanathan, P. P.
MIMO radar space time adaptive processing using prolate spheroidal wave functions.
IEEE Transactions on Signal Processing, **56**, **2** (2008), 623–635.

[10] Willis, N. J., and Griffiths, H. D.
Advances in Bistatic Radar. Raleigh, NC: SciTech Publishing, 2007.

[11] Rouquette, S., and Najim, M.
Estimation of frequencies and damping factors by two-dimensional ESPRIT type methods.
IEEE Transactions on Signal Processing, **49**, 1 (Jan. 2001), 237–245.

[12] Jin, M., Liao, G., and Li, J.
Joint DOD and DOA estimation for bistatic MIMO radar.
Signal Processing, **89**, 2 (2009), 244–251.

[13] Chen, D., Chen, B., and Qin, G.
Angle estimation using ESPRIT in MIMO radar.
Electronics Letters, **44**, 12 (2008), 770–771.

[14] Tang, B., Tang, J., Zhang, Y., and Zheng, Z.
Maximum likelihood estimation of DOD and DOA for bistatic MIMO radar.
Signal Processing, **93**, 5 (2013), 1349–1357.

[15] Chen, J., Gu, H., and Su, W.
Angle estimation using ESPRIT without pairing in MIMO radar.
Electronics Letters, **44**, 24 (2008), 1422–1423.

[16] Bencheikh, M. L., Wang, Y., and He, H.
Polynomial root finding technique for joint DOA DOD estimation in bistatic MIMO radar.
Signal Processing, **90**, 9 (Sep. 2010), 2723–2730.

[17] Xie, R., Liu, Z., and Wu, J.
Direction finding with automatic pairing for bistatic MIMO radar.
Signal Processing, **91**, 1 (2012), 198–203.

[18] Yan, H., Li, J., and Liao, G.
Multitarget identification and localization using bistatic MIMO radar systems.
EURASIP Journal on Advances in Signal Processing (2008), 1–8.

[19] Gershman, A. B., and Sidiropoulos, N. D.
Space-Time Processing for MIMO Communications. New York: Wiley, 2005.

[20] Petersen, K. L., and Sinclair, C. D.
Conjugate reciprocal polynomials with all roots on the unit circle.
Canadian Journal of Mathematics Journal, **60**, 5 (Oct. 2008), 1149–1167.

[21] Zhang, X., Xu, L., and Xu, D.
Direction of departure (DOD) and direction of arrival (DOA) estimation in MIMO radar with reduced-dimension MUSIC.
IEEE Communication Letters, **14**, 12 (2010), 1161–1163.

Frankie K.W. Chan received the B.Eng. degree in computer engineering and the Ph.D. degree in electronic engineering from the City University of Hong Kong in 2002 and 2008, respectively.

He is currently a Research Fellow in the City University of Hong Kong and Shenzhen University. His research interests include parameter estimation, optimization, and distributed processing, with particular attention to frequency estimation, MIMO radar signal processing and node localization in wireless sensor network.

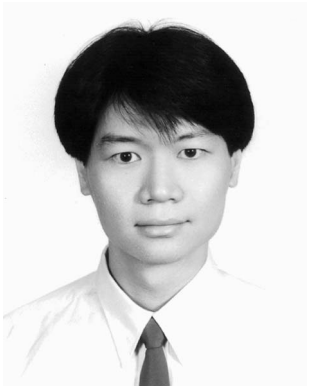

Hing Cheung So (S'90—M'95—SM'07—F'15) was born in Hong Kong. He received the B.Eng. degree from the City University of Hong Kong and the Ph.D. degree from The Chinese University of Hong Kong, both in electronic engineering, in 1990 and 1995, respectively.

From 1990 to 1991, he was an electronic engineer with the Research and Development Division, Everex Systems Engineering Ltd., Hong Kong. During 1995-1996, he worked as a Postdoctoral Fellow with The Chinese University of Hong Kong. From 1996 to 1999, he was a Research Assistant Professor with the Department of Electronic Engineering, City University of Hong Kong, where he is currently an Associate Professor. His research interests include statistical signal processing, fast and adaptive algorithms, signal detection, robust estimation, source localization and sparse approximation. He has been on the editorial boards of *IEEE Signal Processing Magazine* (2014 -), *IEEE Transactions on Signal Processing* (2010 -2014), *Signal Processing* (2010 -), and *Digital Signal Processing* (2011 -). In addition, he is an elected member in Signal Processing Theory and Methods Technical Committee (2011 -) of the IEEE Signal Processing Society where he is also chair in the awards subcommittee (2015 -). He has been elected Fellow of IEEE in recognition of his contributions to spectral analysis and source localization in 2015.

Lei Huang (M'07—SM'14) was born in Guangdong, China. He received the B.Sc., M.Sc., and Ph.D. degrees in electronic engineering from Xidian University, Xi'an, China, in 2000, 2003, and 2005, respectively.

From 2005 to 2006, he was a Research Associate with the Department of Electrical and Computer Engineering, Duke University, Durham, NC. From 2009 to 2010, he was a Research Fellow with the Department of Electronic Engineering, City University of Hong Kong and a Research Associate with the Department of Electronic Engineering, The Chinese University of Hong Kong. From 2011 to 2014, he was a Professor with the Department of Electronic and Information Engineering, Harbin Institute of Technology, Shenzhen Graduate School. Since November 2014, he has joined the Department of Information Engineering, Shenzhen University, where he is currently a Chair Professor. His research interests include spectral estimation, array signal processing, statistical signal processing, and their applications in radar and wireless communication systems.

Dr. Huang is currently an Associate Editor for *IEEE Transactions on Signal Processing* and *Digital Signal Processing*.

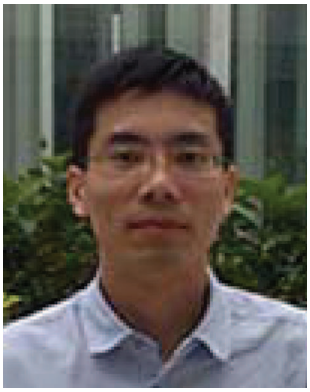

Longting Huang received his M.S. degree in computer science from Wuhan Institute of Technology, China, in 2011. Currently, he is pursuing the PhD. degree in the Department of Electronic Engineering, City University of Hong Kong. His research interests include multidimensional frequency estimation and low-rank matrix / tensor completion.